Electronic Supplementary Material (ESI) for Journal of Materials Chemistry C.


# SUPPLEMENTARY MATERIALS

## Ferroelectricity in Lead Free Organic-Inorganic 0D hybrid:

## Formamidinium Bromoantimonate(III)

K. Mencel[1], A. Gągor[2], R. Jakubas[1], A. Ciżman[3], W. Medycki[4], J. Zaręba[5] and A. Piecha-Bisiorek[1]

*[1] Faculty of Chemistry, University of Wrocław, F. Joliot-Curie 14, 50-383 Wrocław, Poland*
*[2] W. Trzebiatowski Institute of Low Temperature and Structure Research PAS, P.O. Box 1410, 50-950 Wrocław, Poland*
*[3] Department of Experimental Physics, Wrocław University of Science and Technology, Wybrzeże Wyspiańskiego 27, 50-370 Wrocław, Poland*
*[4] Institute of Molecular Physics, Polish Academy of Science, M. Smoluchowskiego 17, 60-179 Poznań, Poland.*

**Table S1.** Phase diagram of $R_5M_2X_{11}$ ferroelectrics.

| Compound | Phase Diagram (FERROELECTRIC / PARAELECTRIC) | $P_s$ [μC/cm²] | $\varepsilon(T_c)$ | Ref. |
|---|---|---|---|---|
| $(MA)_5[Bi_2Cl_{11}]$ | $Pca2_1$ → $Pcab$ at RT, 307 K | 1.2 | 8000 | 1 |
| $(MA)_5[Bi_2Br_{11}]$ | $Pca2_1$ → $Pcab$ at RT, 311 K | 2 | 20000 | 2 |
| $(FA)_5[Sb_2Br_{11}]$ | $P2_1$ → $P2_1/n$ $P2_1/n$ $Pmnn$ at 163 K, 200 K, 233 K, RT | 13 | 55 | Title compound |
| $(PYR)_5[Bi_2Br_{11}]$ | $P2_1$ → $P2_1/n$ at 118 K, RT | 0.3 | 220 | 3 |
| $(IM)_5[Bi_2Cl_{11}]$ | $P2_1$ → $P2_1/n$ → $P4n2$ at 166 K, RT, 360 K | 0.6 | 450 | 4 |
| $(IM)_5[Sb_2Br_{11}]$ | $Pn$ $Pn$ → $P2_1/n$ → $P4n2$ at 120 K, 145 K, RT, 352 K | 0.18 | 250 | 5 |
| $(IM)_5[Bi_2Br_{11}]$ | $Pn$ → ? at 155 K, RT, 352 K | 0.26 | 420 | 6 |

cation: MA-methylammonium, PYR-pyridinium, IM-imidazolium

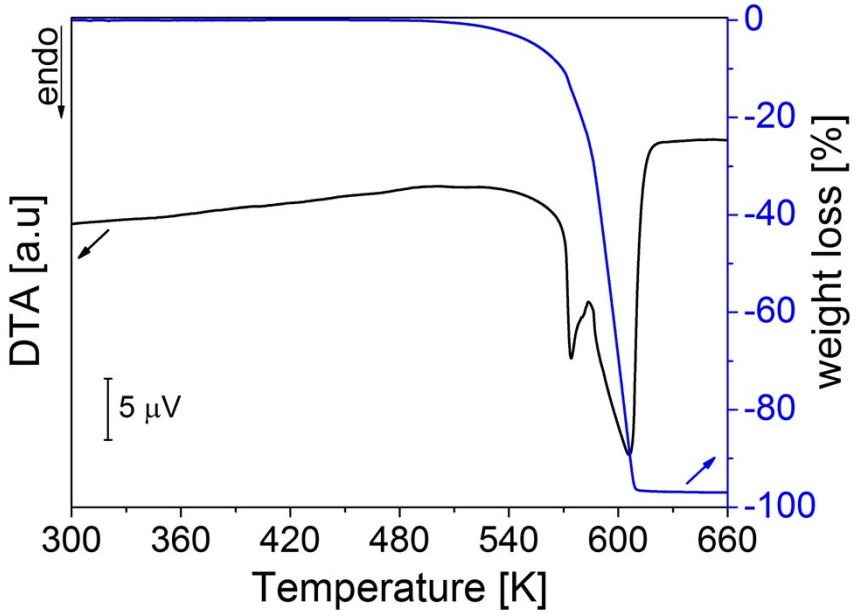


**Figure S1.** Simultaneous thermogravimetric (TGA) and differential thermal analyses (DTA) scan (ramp rate: 5 K $min^{-1}$).

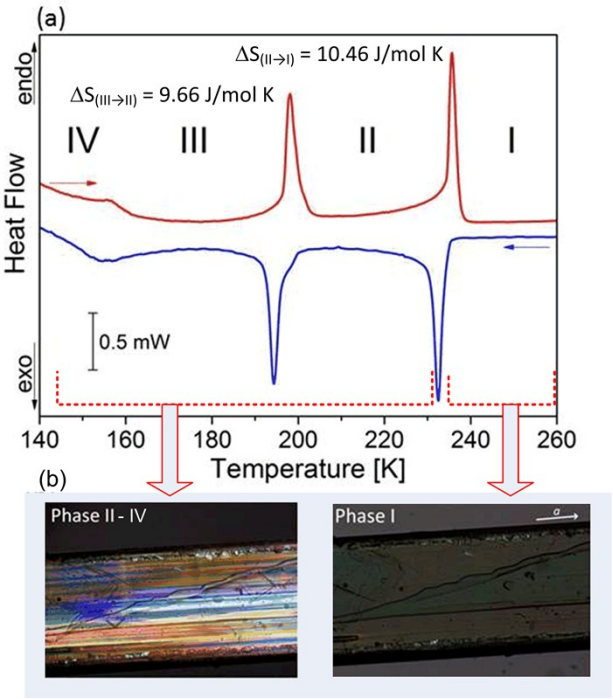


**Figure S2.** **(a)** DSC traces for **FAB** during the cooling and heating scans (rate: 5 K min$^{-1}$, sample mass 12.1220 mg); **(b)** evolution of the ferroelastic domain structure during PT.

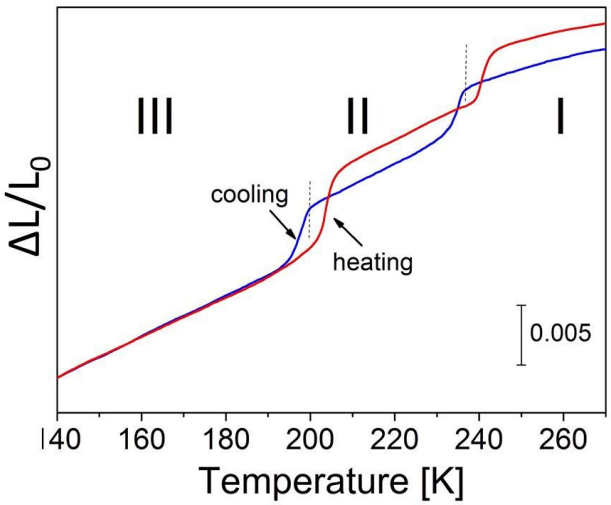


**Figure S3.** Thermal expansion along the *a*-axis (the scanning rate of 3 K min$^{-1}$).

In order to verify the sequence and character of these structural transformations, dilatometric measurement was performed (see Figure S3). The obtained results are consistent with the calorimetric studies (discontinuous character of transitions from **I→II**, **II→III** and continuous for the lowest one (**III→IV**)). The high temperature PTs are accompanied by a step-like change of the linear thermal expansion ($\Delta L/L_0$), characteristic for a discontinuous transformation. In the case of a PT at 163 K, the anomaly is hardly visible - only very subtle inflection of the baseline can be observed, which confirms a continuous type of this PT.

**Table S2.** Experimental details.

| | 250 K | 220 K | 180 K | 100 K |
|---|---|---|---|---|
| ***Crystal data*** | | | | |
| Crystal system, space group | Orthorhombic, *Pmnn* | Monoclinic, $P2_1/n$ | Monoclinic, $P2_1/c$ | Monoclinic, $P2_1$ |
| Temperature (K) | 250 | 220 | 180 | 100 |
| *a*, *b*, *c* (Å) | 8.5458 (4), 14.2043 (7), 13.6227 (7) | 8.5603 (6), 14.3249 (12), 13.2890 (13) | 16.2457 (12), 14.2267 (8), 15.1237 (11) | 16.2118 (9), 14.1972 (4), 14.9780 (7) |
| α, β, γ (°) | 90, 90, 90 | 90, 93.542 (7), 90 | 90, 113.536 (9), 90 | 90, 112.787 (5), 90 |
| *V* (Å$^3$) | 1653.61 (15) | 1626.5 (2) | 3204.6 (4) | 3178.3 (3) |
| *Z* | 2 | 2 | 4 | 4 |
| Crystal size (mm) | 0.21 × 0.16 × 0.13 | 0.21 × 0.16 × 0.13 | 0.21 × 0.16 × 0.13 | 0.21 × 0.16 × 0.13 |
| ***Data collection*** | | | | |
| $T_{min}$, $T_{max}$ | 0.519, 1.000 | 0.627, 1.000 | 0.668, 1.000 | 0.710, 1.000 |
| No. of measured, independent and observed [$I > 2\sigma(I)$] reflections | 6789, 1682, 962 | 6105, 6105, 2982 | 9778, 9775, 5896 | 10039, 10039, 7615 |
| $(\sin\theta/\lambda)_{max}$ (Å$^{-1}$) | 0.610 | 0.693 | 0.610 | 0.610 |
| Refinement | | | | |
| $R[F^2 > 2\sigma(F^2)]$, $wR(F^2)$, *S* | 0.056, 0.190, 0.95 | 0.054, 0.130, 0.88 | 0.043, 0.102, 0.82 | 0.066, 0.193, 0.98 |
| No. of reflections | 1682 | 6105 | 9775 | 10037 |
| No. of parameters | 62 | 93 | 238 | 488 |
| No. of restraints | 11 | 9 | 19 | 201 |
| H-atom treatment | H-atom parameters not defined | H-atom parameters constrained | H-atom parameters constrained | H-atom parameters constrained |
| $\Delta\rho_{max}$, $\Delta\rho_{min}$ (e Å$^{-3}$) | 0.900, -0.863 | 1.56, -0.93 | 1.73, -1.39 | 3.36, -2.125 |
| Absolute structure | – | – | – | Classical Flack method preferred over Parsons because s.u. lower. |
| Absolute structure parameter | – | – | – | 0.50 (2) |

Computer programs: *CrysAlis PRO* 1.171.38.43 (Rigaku OD, 2015), *SHELXL2018*/3 (Sheldrick, 2018). **Pnmm* in the standard setting.

**Table S3.** Geometrical parameters of $[Sb_2Br_{11}]^{5-}$ anions, selected interatomic distances, angles, Δd - bond length distortion; $\sigma^2$ octahedral angle variance [7].

| Phase | Sb-Br | Δdx10$^3$ | Br-Sb-Br$_{cis}$ | Br-Sb-Br$_{trans}$ | σ (°) |
|---|---|---|---|---|---|
| **I** | 2.616(2)-3.048(1) | 2.3 | 89.6-91.7 | 177.9-179.3 | 0.96 |
| **II** | 2.612(2)-3.046(1) | 3.0 | 87.4-92.2 | 176.5-179.1 | 1.89 |
| **III** | 2.643(2)-2.989 (2) | 2.6 | 85.0-92.5 | 175.4-177.5 | 3.98 |
| | 2.598 (2)-3.091(2) | 4.7 | 87.4-94.6 | 173.4-175.9 | 5.90 |
| **IV** | 2.621(5)- 3.059(5) | 3.4 | 83.3-94.6 | 172.6-177.9 | 8.53 |
| | 2.594(5) -3.048(5) | 5.1 | 88.9-94.1 | 175.7-176.8 | 4.69 |
| | 2.639(4) -2.999(5) | 2.7 | 84.8-92.1 | 176.2-179.2 | 4.42 |
| | 2.601(5)- 3.033(5) | 5.4 | 84.2-95.1 | 171.8-173.7 | 13.32 |

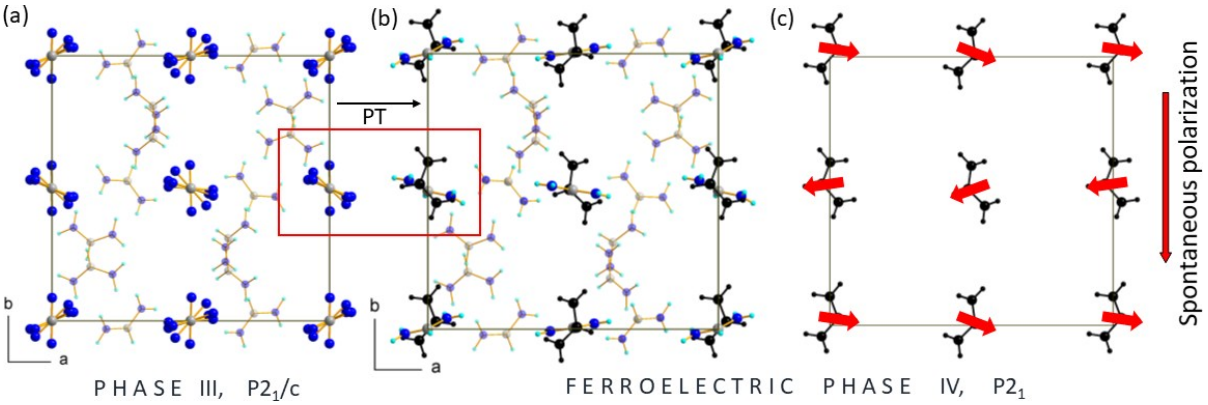


**Figure S4**. Ordering of polar $FA^+$ gives substantial contribution to the polar properties of **FAB (a)** presents the cations in non-polar Phase **III**, disordered $FA^+$ are highlighted; **(b)** shows ordered positons of $FA^+$ in ferroelectric phase **IV**; **(c)** the dipole moments of ordered cations give resultant polarization along the *b*-axis.

## Dielectric properties

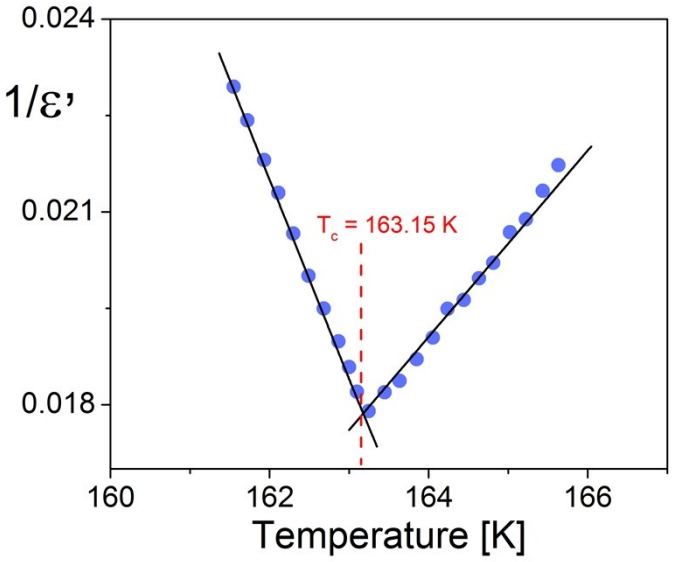


**Figure S5.** The Curie-Weiss law of ferroelectricity (1/ε') at 135 Hz.

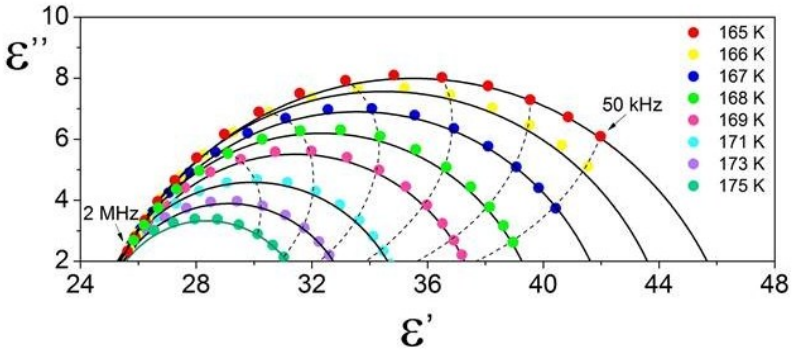


| T [K] | α | τ * 10$^6$ |
|---|---|---|
| 175 | 0.0230 | 0.154 |
| 173 | 0.0587 | 0.196 |
| 171 | 0.0978 | 0.253 |
| 169 | 0.0928 | 0.400 |
| 167 | 0.1311 | 0.679 |
| 166 | 0.2001 | 0.831 |
| 165 | 0.2223 | 1.210 |

**Figure S6.** The Cole-Cole plots and the fit parameters of the relaxation process.

The dielectric relaxation process is well described by the following Cole–Cole relation:

$$\varepsilon^*(\omega) = \varepsilon_\infty + \frac{\varepsilon_0 - \varepsilon_\infty}{1 + (i\omega\tau)^{1-\alpha}}$$

where: $\varepsilon_0$ and $\varepsilon_\infty$ are the low and high frequency limits of electric permittivity, respectively, $\omega$ is the angular frequency, and $\tau$ is the macroscopic relaxation time.

The obtained Cole-Cole plots are presented in Figure S6. All parameters ($\varepsilon_0$, $\varepsilon_\infty$, $\tau$ and $\alpha$) at selected temperatures were estimated by using the results of $\varepsilon^*(\omega)$ at several frequencies between 50 kHz and 2 MHz. The fit parameters of the relaxation process are listed in the right-hand of the Fig. S7. As it is shown, the Cole-Cole plots deviate slightly from semi-circles at temperatures from 175 K to 167 K. Taking into account the small value of $\alpha$ (~0.02-0.13) over this temperature range, it indicates that a monodispersive relaxation process in the title crystal takes place. However, upon approaching $T_c$ in the paraelectric phase **III**, the $\alpha$ parameter increases up to 0.2 suggesting a polidispersive character of the relaxation process. Although it is well known from literature that most ferroelectrics exhibit monodispersive properties (even in the close vicinity of $T_c$), in some ferroelectrics, the appearance of the distribution of relaxation times may be due to the temperature fluctuation in the sample. Therefore, the distribution of macroscopic relaxation times in **FAB** we explained either as the presence of two dielectric relaxation process (two kinds of dynamically disordered dipolar formamidinium cations) or as a result of the temperature gradient on the sample.

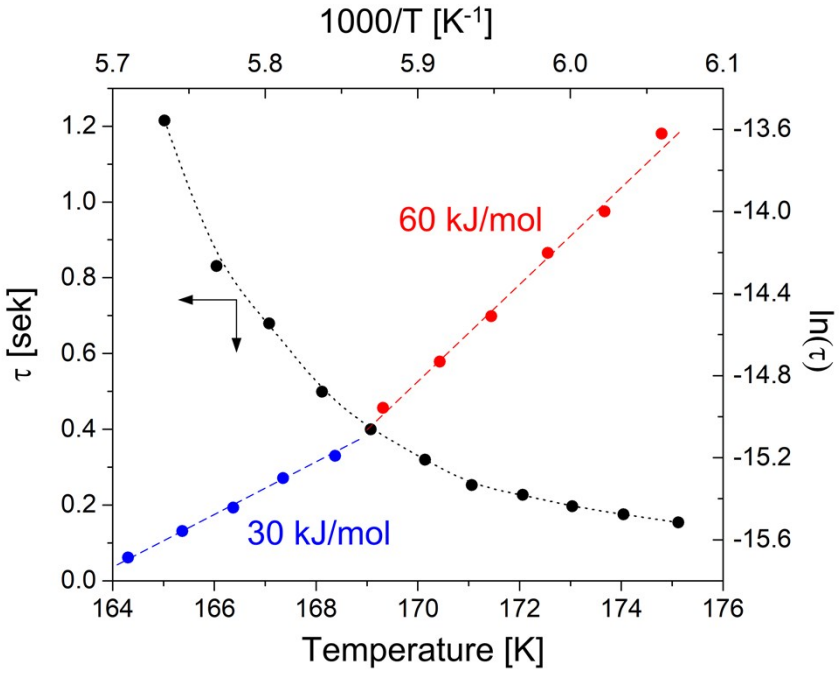


**Figure S8**. Temperature dependence of $\tau$ versus temperature and $\ln(\tau)$ versus reciprocal temperature for **FAB**.

To confirm the ferroelectric properties of **FAB** the pyroelectric measurements were undertaken. The pyroelectric current was measured after poling the crystal while cooling from 200 K down to about 100 K. The dc electric field was equal to +5 kV·cm$^{-1}$. Then the pyroelectric current, ($I_{pyro}$) was measured during the heating cycle. The same procedure was applied after poling the crystal by a dc electric field of negative value -5 kV·cm$^{-1}$ (see Fig. S9(a)). The calculated spontaneous polarization $P_s$ plotted as a function of temperature is shown in Figure S9(b). The spontaneous polarization ($P_s$) is reversed by the external dc electric field which is a crucial evidence of ferroelectric properties below 163 K. The $P_s$ value is found to be about 0.2 μC·cm$^{-2}$ at 140 K (Figure S9(b)).

One should note that the value of $P_s$ obtained from pyroelectric current measurement is significantly lower in comparison with hysteresis loop measurements (≈3 μC·cm$^{-2}$; Figure 3(b)). This result, in our opinion, is related to the fact that due to the distinct coercive field the obtained value of polarization was not saturated.

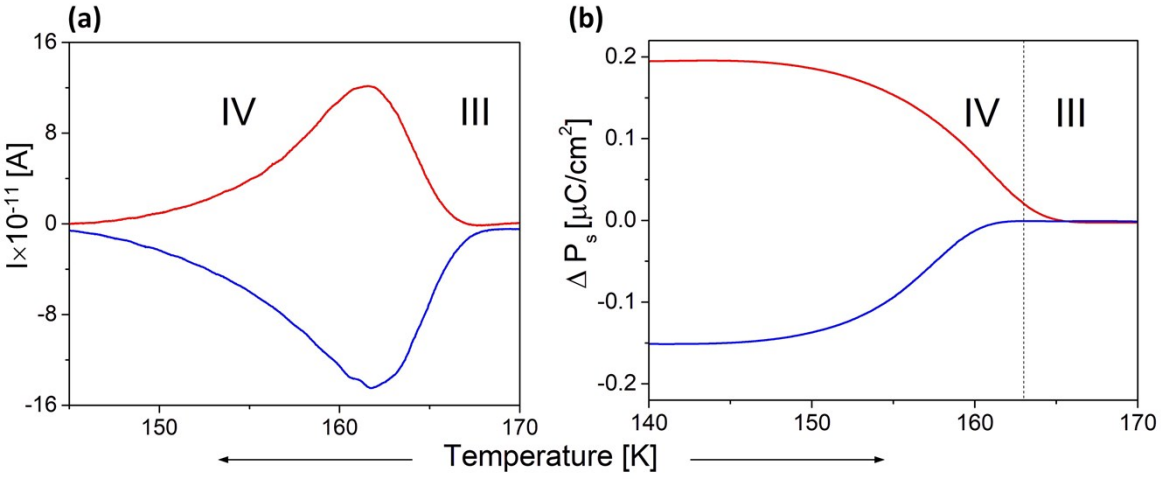


**Figure S9**. (a) Temperature dependence of $I_{pyro}$; (b) Spontaneous polarization ($P_s$) as a function of temperature from the pyroelectric effect for the poling electric field ±5 kV cm$^{-1}$ for **FAB (**polycrystalline (pressed) samples).

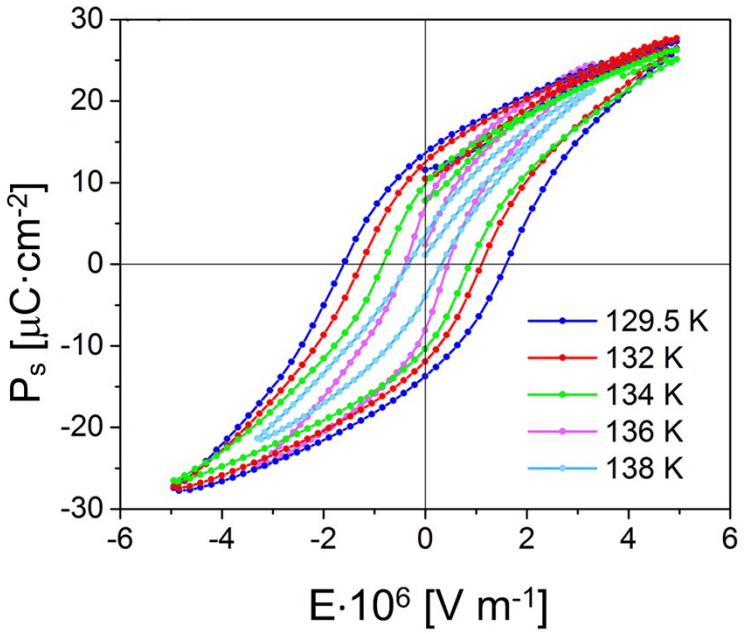


**Figure S10**. Hysteresis loops measured at several temperatures for the single crystal sample (along *b*-axis).

## $^1$H NMR ($T_1$ spin lattice, $M_2$- second moment) measurements.

The measurements of the temperature dependencies of the proton nuclear relaxation time $T_1$ for **FAB** are shown in Fig. S11(a). Two different temperature ranges can be distinguished. In the lowest temperatures, below 110 K, the nearly constant values of longitudinal relaxation times are observed form 1.7 s to 1.3 s. Such small changes, however, long $T_1$ relaxation times may denote the domination of the quadrupole interaction [8,9] in the lowest temperatures reached in the present study. Next, the unsymmetrical minimum of relaxation times is visible with $T_{1min}$ = 70 ms at 200 K. Three detected PTs at 163, 201 and 233 K weakly reflected in measured temperature dependencies of $T_1$ times. This may mean that these PTs are more the result of changes in the molecular dynamics of anions. The double minimum originates from relaxation of two in-equivalent formamidinium cations. The measured points we fit with BPP theory using the following formula [10,11]:

$$\frac{1}{T_1} = C_1 \frac{\tau_{c1}}{1+\omega^2\tau_{c1}^2} + \frac{4\tau_{c1}}{1+4\omega^2\tau_{c1}^2} + C_2 \frac{\tau_{c2}}{1+\omega^2\tau_{c2}^2} + \frac{4\tau_{c2}}{1+4\omega^2\tau_{c2}^2}$$

In this equation ω represents the Larmor resonance angular frequency, $C_1$ and $C_2$ – relaxation constants and the $\tau_{c1}$ and $\tau_{c2}$ are the correlation times for both formamidinium in-equivalent cations, respectively. The temperature dependence of correlation time is described by the Arrhenius law: $\tau_{ci}=\tau_{oi}\exp(E_a/RT)$, where $\tau_{0i}$ is the correlation time at the limit infinite temperature, $E_a$ – the height of the barrier, R – gas constant. The obtained fitting parameters are collected in Table S4. These parameters indicate the standard process relaxation for one from two different types of in-equivalent formamidinium cations but the second type has value of the correlation time that is rather atypically low. Such low values of the correlation time we previously found, for example, in compounds bearing cyclic cations [12].

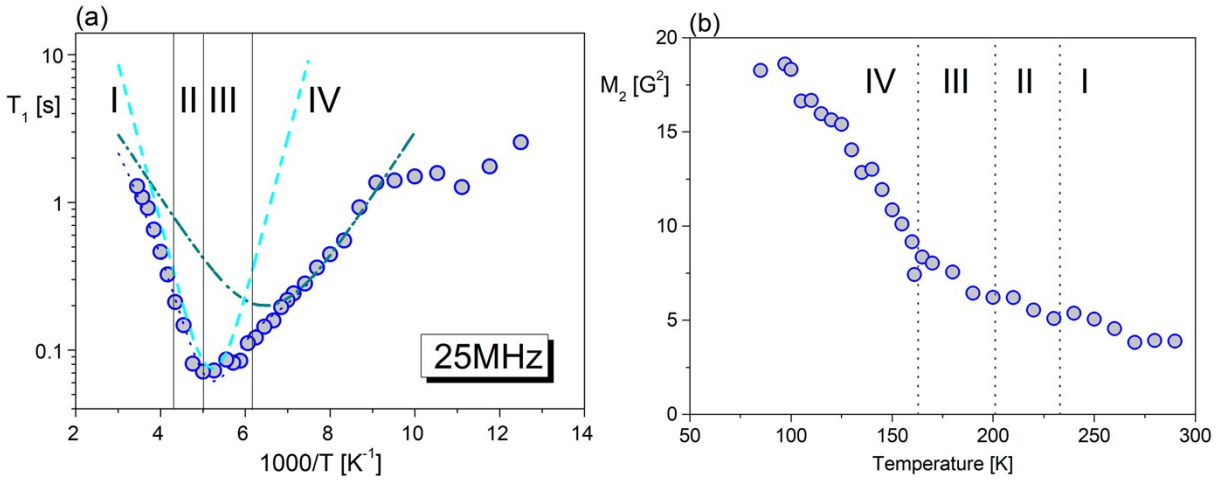


**Figure S11**. Temperature dependence of (a) spin-lattice relaxation times ($T_1$) for protons, at 25 MHz; (b) $^1$H NMR second moment ($M_2$) of **FAB**.

The second-moment of $^1$H NMR line for **FAB** sample (Fig. S11(b)) shows that from lowest temperatures up to the temperature of the first phase transition at 163 K occurs the continuous reduction of the second moment value from about 18.5 $G^2$ to 8.4 $G^2$. Then the observed reduction is much weaker and at room temperature the second moment drops to 3.9 $G^2$. Such a temperature dependence of the second moment is different than previously found for already published study of the formamidinium iodide (FAI) [13]. For **FAI** in lowest temperatures the plateau- the characteristic for rigid state- has been found and in 420 K the second moment drops below 1 $G^2$. In studied here **FAB** the rigid state has been not reached in the lowest temperatures and at room temperature axial reorientation of formamidinium cation still occurs before expected final tumbling at higher temperatures.

**Table S4**. The fitting parameters of the relaxation process.

| Parameter | **FAB** |
|---|---|
| $E_{a1}$ [kcal/mol] | 1.98 |
| $\tau_{01}$ [s] | $6.3\ 10^{-12}$ |
| $C_1$ [$s^{-2}$] | $5.5\ 10^{9}$ |
| $E_{a2}$ [kcal/mol] | 4.94 |
| $\tau_{02}$ [s] | $8.9\ 10^{-15}$ |
| $C_2$ [$s^{-2}$] | $1.47\ 10^{9}$ |


1. J. Lefebvre, P. Carpentier and R. Jakubas, Acta Cryst., 1991, B47, 228.
2. J. Matuszewski, R. Jakubas, L. Sobczyk and T. Głowiak, Acta Cryst., 1990, C46, 1385.
3. J. Jóźków, R. Jakubas, G. Bator and A. Pietraszko, J. Chem. Phys., 2001, 114, 7239.
4. R. Jakubas, A. Piecha, A. Pietraszko and G. Bator, Phys. Rev., 2005, B72, 104107.
5. A. Piecha, A. Pietraszko, G. Bator and R. Jakubas, J. Solid State Chem., 2008, 181, 1155.
6. A Piecha, A Białońska and R Jakubas, J. Phys.: Condens. Matter, 2008, 20, 325224.
7. M.E. Fleet, Mineral. Mag., 1976, 40, 531.

8. P. Szklarz, J. Zaleski, R. Jakubas, G. Bator, W. Medycki and K. Falińska, J. Phys.: Condens. Matter, 2005, 17, 2509.
9. A. Piecha, R. Jakubas, A. Pietraszko, J. Baran, W. Medycki and D. Kruk, J. Solid State Chem., 2009, 182, 2949.
10. N. Bloembergen, E.M. Purcell and R. V. Pound, Phys. Rev., 1948, 73, 679.
11. A. Piecha, A. Gągor, M. Węcławik, R. Jakubas and W. Medycki, Mater. Res. Bull., 2013, 48, 151.
12. A. Piecha, A. Białońska, R. Jakubas and W. Medycki, Solid State Sci., 2008, 10, 1469.
13. K. Mencel, P. Durlak, M. Rok, R. Jakubas, J. Baran, W. Medycki, A. Ciżman and A. Piecha-Bisiorek, RSC Adv., 2018, 8, 26506.